*J. Fluid Mech.* (1974), *vol.* 62, *part* 3, *pp.* 417–436
*Printed in Great Britain*



# The effect of side walls on homogeneous rotating flow over two-dimensional obstacles

By HERBERT E. HUPPERT
Department of Applied Mathematics and Theoretical Physics, University of Cambridge

AND MELVIN E. STERN
Graduate School of Oceanography, University of Rhode Island, Kingston, Rhode Island 02881

(Received 25 May 1973)

We consider the flow of a slightly viscous homogeneous fluid over a small two-dimensional obstacle perpendicular to the vertical side walls in a channel rotating about a vertical axis. The flow in the channel is obtained from the solution of the quasi-geostrophic potential vorticity equation in the limit $\epsilon = D/L \to 0$, where $D$ is the obstacle width and $L$ the channel width. The lowest order, interior flow is shown to be a combination of three effects: a rotational flow caused by vortex stretching and Ekman boundary-layer pumping; a significant irrotational flow induced by the magnitude of the former flow at the vertical boundaries; and the interior Ekman drift due to the basic current. The maximum streamline displacement is calculated and compares very well with recent experiments in the identical parameter range by Boyer (1971*a*, *b*). This theory explains how the side walls are responsible for the dependence of the maximum streamline displacement on Rossby number.

## 1. Introduction

One of the major motivations behind the fluid dynamiscist's interest in rotating flows is due to the important role of rotation and the accompanying Coriolis force in determining many of the fluid motions in the atmosphere and the ocean. Theoretical considerations, laboratory experiments and large scale, geophysical measurements have all contributed to our present understanding of rotating fluids, although the developments in these somewhat separate areas have not always been co-ordinated. Recently, Boyer (1971*a*,*b*) presented the results of two different experiments involving the flow of a homogeneous fluid over a variable bottom, which were designed specifically to confirm the applicability of his accompanying analysis. Investigations such as those of Boyer are interesting and may be useful in modelling many geophysically significant situations. Boyer & Guala (1972) have extended Boyer's original study to consider the Antarctic Circumpolar Current near the Macquarie ridge, and in many other areas of the ocean, investigations of the interactions between currents and bottom topography are needed. We are primarily concerned here, however, with Boyer's original experiments.

A viscous homogeneous fluid flows over an obstacle of constant cross-section whose breadth, say $D$, is very much less than its length, say $L$. The system rotates at a constant angular velocity, say $\Omega$, about a vertical axis such that the Ekman number is

$$E = \nu/(2\Omega D^2) \ll 1, \tag{1.1a,b}$$

the Rossby number is

$$R = U/(2\Omega D) \sim E^{\frac{1}{2}} \tag{1.2a,b}$$

and the maximum height of the obstacle is

$$h_0 \sim DE^{\frac{1}{2}}, \tag{1.3}$$

where $U$ is the magnitude of the current far upstream in the interior of the flow, outside any boundary layers. Figure 1 is a sketch of the system. Boyer's experiments and resulting theory were actually undertaken for the flow between two obstacles, attached symmetrically to two infinite, horizontal planes separated by a distance $2H$, very much greater than $2h_0$. This configuration makes the centre-plane enjoy a convenient symmetry, which is exploited in the analysis and removes the influence of the Ekman layers on the horizontal rigid lid that might have been used instead. Alternatively, the system can be viewed as the free-surface (stress-free) flow of fluid of depth $H$ over one obstacle. In the following it is only this lower portion of the total flow which is investigated, the flow in the upper portion being obtainable by reflexion. Boyer's original analysis (1971*a*) is directed towards considering obstacles with continuous cross-sectional profiles, triangles for example, while his later work (1971*b*) is undertaken to describe the flow over a rectangle. In both cases the analysis allows for the interior flow far upstream to be at an angle, say $\alpha$, to the obstacle, although quantitative experimental results are presented only for $\alpha = 0$. Therefore we consider only this case, for which figure 1 indicates the co-ordinate system to be used.

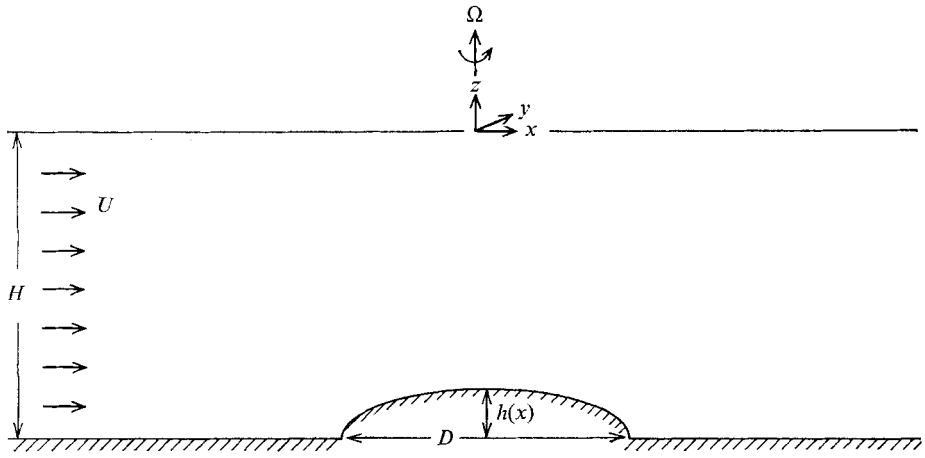


FIGURE 1. An elevation of the channel which has vertical walls at $y = \pm \frac{1}{2}L$.

Under conditions (1.1)–(1.3) the flow is quasi-geostrophic and is determined by a balance between the nonlinear inertial effects, Ekman boundary-layer

pumping and topographic stretching of vertical columns [see equation (2.1)]. As the fluid flows over the obstacle, the interior relative vorticity, i.e. the interior vorticity relative to co-ordinates fixed in the rotating frame, is altered by the change in length of vortex filaments as they go over the obstacle, while the magnitude of the vorticity is decreased by Ekman-layer pumping. If the flow is two-dimensional, inviscid and $h_0 \sim R$, the streamlines in the interior of the flow, which are independent of height, are straight until they are over the obstacle. They then turn in a readily calculable manner to leave the region over the obstacle in a straight line making an angle

$$\tan^{-1}(2\Omega A_*/HU)$$

to the right† with the original direction, where $A_*$ is the cross-sectional area of the obstacle. The addition of viscosity will clearly alter this result. In what manner? It is to this question that Boyer addresses himself. In particular, he seeks to determine the orientation between the same streamline far upstream and far downstream.

To do this Boyer uses an $E^{\frac{1}{2}}$ power-series expansion, retains only the first non-zero terms and assumes that the flow does not vary in the $y$ direction. His calculation shows that the streamlines are straight and parallel far upstream of the obstacle and also sufficiently far downstream. In passing over the obstacle the columns of fluid are displaced to the right by an amount

$$S_* = \begin{cases} 2^{-\frac{1}{2}} h_0 E^{-\frac{1}{2}} & \text{for a triangle,} \quad (1.4) \\ 2^{\frac{1}{2}} h_0 E^{-\frac{1}{2}} & \text{for a rectangle.} \quad (1.5) \end{cases}$$

Boyer notes the rather surprising absence of the Rossby number in these results but does not explain its absence other than to say that the streamline displacement would appear to be independent of the inertial effects. Comparing these results with measurements made in the centre of the channel, Boyer finds a fairly strong dependence of streamline displacement on Rossby number, even though conditions (1.1)–(1.3) are satisfied. The experimental results indicate that the displacement decreases monotonically with increasing Rossby number as shown in figures 2–5. Even for the comparatively small Rossby number of 0·1 the measured displacement is over $\frac{1}{3}$ less than his two-dimensional theory predicts. The purpose of this paper is to explain the observed disagreement.

Boyer suggests that the discrepancy might be obviated by continuing his expansion, thereby including terms of higher order in the Rossby number. It is essential to investigate whether this idea is correct; the implication would be that calculations for even quite small Rossby numbers would have to be taken to second order if reasonable accuracy is required. The suggestion, however, does not appear to be correct, since as is proved in § 3, the effect of the next-order term on the far-downstream streamline displacement is zero. Thus, given the assumptions made by Boyer, the results (1.4) and (1.5) have errors at most of order $R^2$ which is far too small to explain the discrepancy.

† Here, and elsewhere, 'left' and 'right' are with reference to an observer looking in the downstream direction.

As we show below, it is possible to obtain in five lines [equations (2.1) and (2.20)–(2.23)] the general result

$$S_* = 2^{\frac{1}{2}} A_* E^{-\frac{1}{2}}/D, \tag{1.6}$$

of which (1.4) and (1.5) are particular cases. The situation can be made to appear even more problematic by continuing the analysis further, (2.24)–(2.31), from which it appears that a full, three-dimensional calculation, incorporating the two vertical walls that are present at the ends of the obstacle, leads to

$$S_* = 0 \tag{1.7}$$

*no matter how far apart the walls are.*

Part of the explanation of the discrepancy between Boyer's experiment and theory can be obtained by a careful interpretation of (1.7). We show in § 2 that the solution of the zeroth-order vorticity equation which takes into account the existence of the two end walls predicts that an interior streamline gently drifts to the left upstream of the obstacle. It then veers sharply to the right above, and for some distance downstream of, the obstacle, coming to a position of maximum displacement with respect to its position at the upstream edge of the obstacle. There is then a gentle drift to the left again, the final downstream position being in line with the upstream one, in accordance with (1.7). Asserting that it is the *maximum* displacement which Boyer measured,† we calculate a streamline displacement which does vary with Rossby number in the same manner as is experimentally observed and presented in figures 2–5.

Although qualitatively correct – the predicted streamline displacement decreases with increasing Rossby number – the agreement between the theory of § 2 and Boyer's experimental results is quantitatively only fair. The reason for this is shown in § 3 to be because the theory of § 2 tacitly assumes that

$$\epsilon \equiv D/L \gg E^{\frac{1}{2}}. \tag{1.8}$$

In Boyer's experiment $\epsilon \sim E^{\frac{1}{2}}$ and it is shown in § 3 how to calculate the maximum streamline displacement taking this into account. The additional feature thereby incorporated which affects the results is the $O(E^{\frac{1}{2}})$ Ekman drift in the interior of the channel. The maximum streamline displacement so calculated, and presented in figures 2–5, now agrees well with the experimental measurements.

## 2. The simplest theory incorporating end walls

The lowest order vorticity equation relevant to the system described in § 1 and sketched in figure 1 with the obstacle represented by $h(x)$ is (Ingersoll 1969, § 2)

$$\mathbf{q} \cdot \nabla \left( \zeta + \frac{2\Omega}{H} h \right) + \frac{(\Omega\nu)^{\frac{1}{2}}}{H} \zeta = 0, \tag{2.1}$$

where $\mathbf{q}$ is the interior, depth-independent, horizontal velocity vector,

$$\mathbf{q} = (u, v) \tag{2.2}$$

† Boyer (private communication) agrees with this.

and $\zeta$ is the vertical component of relative vorticity given by

$$\zeta = v_x - u_y. \tag{2.3}$$

The vertical velocity $w$ is absent from the $\mathbf{q}.\nabla$ operator in (2.1) because $w$ is $O(E^{\frac{1}{2}})$, in contrast to $u$ and $v$, which are $O(1)$, and hence does not appear in the lowest order equation. The first term in (2.1) represents the rate of change of relative vorticity following the motion. This change is caused by topographic stretching, represented by the second term, and Ekman-layer pumping, represented by the third term. The coefficient $(\Omega\nu)^{\frac{1}{2}} H^{-1}$ of the third term is the inverse of the spin-up time (Greenspan 1968; Greenspan & Howard 1963).

Since the flow is geostrophic to leading order

$$u = -(2\Omega)^{-1} P_y, \quad v = (2\Omega)^{-1} P_x, \tag{2.4), (2.5}$$

where $P$ is the dynamic pressure (total pressure minus the hydrostatic pressure due to gravitational and centrifugal accelerations) divided by the (constant) density $\rho$. From (2.4) and (2.5) we see that $P$ is proportional to the stream function for the (horizontal) motion and is related to the vorticity by

$$\zeta = (2\Omega)^{-1} \nabla^2 P. \tag{2.6}$$

We now find it convenient to introduce the function $S(x, y)$ that represents the displacement in the cross-channel direction of the streamline which originated at $(-\infty, y)$. It follows from this definition that $S$ is related to the velocity components by

$$v = uS_x. \tag{2.7}$$

Comparing (2.7) and (2.5), we determine that

$$P = 2\Omega \int_{-\infty}^{x} uS_x \, dx - 2\Omega U y \tag{2.8}$$

and hence that

$$\zeta = \nabla^2 \int_{-\infty}^{x} uS_x \, dx, \tag{2.9}$$

where we have used the fact that $P \to -2\Omega U y$ as $x \to -\infty$ in deriving (2.8). Substituting (2.9) into (2.1), we obtain

$$\mathbf{q}.\nabla \left[ \nabla^2 \int_{-\infty}^{x} uS_x \, dx + \frac{2\Omega}{H} h \right] + \frac{(\Omega\nu)^{\frac{1}{2}}}{H} \nabla^2 \int_{-\infty}^{x} uS_x \, dx = 0. \tag{2.10}$$

Since both the velocity components and $S$ are unknown and to be determined, (2.10) is quite strongly nonlinear. The simplest, linearized version of (2.10), obtained by setting $u = U$ and $\mathbf{q}.\nabla = U\delta_x$, is

$$\partial_x \left( U \nabla^2 S + \frac{2\Omega}{H} h \right) + \frac{(\Omega\nu)^{\frac{1}{2}}}{H} \nabla^2 S = 0. \tag{2.11}$$

In the remainder of this section, we determine the appropriate solution of (2.11) and present in the appendix an *a posteriori* consistency calculation to indicate that (2.11) is a valid approximation of (2.10) with an error that is uniformly $O(\epsilon)$.

Rather than deal with (2.11) directly, we introduce non-dimensional coordinates $\xi$ and $\eta$ and the non-dimensional functions $M(\xi)$ and $\sigma(\xi,\eta)$ defined by

$$x = \tfrac{1}{2}D\xi, \quad y = \tfrac{1}{2}L\eta, \quad h(x) = h_0 M(\xi) \quad (2.12), (2.13), (2.14)$$

and

$$S(x,y) = -(2E)^{-\frac{1}{2}} h_0 \sigma(\xi,\eta). \tag{2.15}$$

The obstacle is now represented by $M(\xi)$, a function of maximum value 1 with support on $\xi = [-1, 1]$. Substituting (2.12)–(2.15) into (2.11), we obtain

$$(N\partial_\xi + 1)(\partial^2_{\xi\xi} + \epsilon^2 \partial^2_{\eta\eta})\,\sigma(\xi,\eta) = M'(\xi), \tag{2.16}$$

where

$$N = 2^{\frac{3}{2}} \frac{RH}{E^{\frac{1}{2}}D} \tag{2.17}$$

is, by hypothesis, of order 1 with respect to $E$. To (2.16) must be added the boundary conditions that a streamline originating on a wall remains on that wall, that is

$$\sigma(\xi, \pm 1) = 0, \tag{2.18$a,b$}$$

and that, from the definition of $S(x,y)$,

$$\sigma(\xi,\eta) \to 0 \quad (\xi \to -\infty). \tag{2.19}$$

In writing down (2.18) we have neglected the effects of vertical boundary layers of thickness $E^{\frac{1}{4}}$ on the end walls, which is justified for this lowest order analysis.

The solution of (2.16) is most conveniently obtained by expressing $\sigma\,(\xi,\eta)$ as

$$\sigma(\xi,\eta) = \sigma_0(\xi) - \sigma_1(\xi,\eta), \tag{2.20}$$

where $\sigma_0(\xi)$ is the two-dimensional solution for an infinitely long obstacle and satisfies

$$(N\partial_\xi + 1)\,\partial^2_{\xi\xi}\sigma_0 = M'(\xi). \tag{2.21}$$

Equation (2.21) can be deduced directly from (2.1) or (2.10) without making the linearization (2.11).

Integrating (2.21) twice using (2.19) leads to

$$(N\partial_\xi + 1)\,\partial_\xi \sigma_0 = M(\xi), \tag{2.22}$$

$$(N\partial_\xi + 1)\,\sigma_0 = \int_{-\infty}^{\xi} M(t)\,dt, \tag{2.23}$$

from which we see that

$$\sigma_0(\infty) = \int_{-\infty}^{\infty} M(t)\,dt = A, \quad \text{say}, \tag{2.24$a,b$}$$

which is the non-dimensional version of (1.6) and is independent of $N$, or the Rossby number.

This two-dimensional solution represents a flow which is constant in both magnitude and direction upstream of the obstacle, arriving at the upstream edge at right angles to it, with speed $U$ and zero relative vorticity. As the flow mounts the obstacle (assuming $h(x)$ to be non-negative), the vortex filaments are compressed, inducing negative vorticity which is decreased by Ekman-layer pumping, and the flow turns to the right. When the flow has passed the crest of

the obstacle, positive vorticity is induced by topographic stretching of the vortex filaments and negative vorticity is induced by Ekman-layer pumping. Because of viscous effects, the flow arrives at the downstream edge of the obstacle with negative vorticity, which for the remainder of the downstream flow is brought to zero solely by Ekman-layer pumping. In this region of the flow the rate of change of vorticity is proportional to the vorticity itself and therefore the rate of change of the cross-stream velocity is proportional to the cross-stream velocity itself. Thus, the only possible final state is one of zero cross-stream velocity, that is, with the streamlines parallel to their original direction. This final state must be independent of $U$, which enters only in determining how rapidly the flow passes the obstacle and not in the essentials of the dynamics. Therefore, the net streamline displacement must be independent of Rossby number, the only external quantity containing $U$.

If the flow is effectively inviscid, Ekman-layer pumping is absent and since equal amounts of vortex compression and stretching occur as the fluid flows over the obstacle, it arrives at the downstream edge with zero relative vorticity and continues downstream in this state. However, as the fluid flows over the obstacle, the change in vorticity means that there is a continual increase in negative $y$-velocity. The value at the downstream edge of this velocity is hence also retained and the flow continues at the angle

$$\tan^{-1}(2\Omega A_*/HU)$$

to the right from its original direction.

Turning now to the evaluation of $\sigma_1(\xi, \eta)$, we substitute (2.20) into (2.16), (2.18) and (2.19) and use the definition (2.21) for $\sigma_0$ to find that $\sigma_1(\xi, \eta)$ satisfies

$$(\partial_{\xi\xi} + \epsilon^2 \partial_{\eta\eta})\,\sigma_1 = 0, \tag{2.25}$$

$$\sigma_1(\xi, \pm 1) = \sigma_0(\xi), \tag{2.26a,b}$$

$$\sigma_1(\xi, \eta) \to 0 \quad (\xi \to -\infty). \tag{2.27}$$

Thus, the decomposition (2.20) states that the total flow can be considered as the sum of a two-dimensional rotational flow induced by the presence of the obstacle and Ekman-layer pumping plus a three-dimensional rotational flow induced entirely by the value of the previous part at the boundary. Sufficiently far downstream (2.25) and (2.26) become

$$\epsilon^2 \partial_{\eta\eta} \sigma_1 = 0, \tag{2.28}$$

$$\sigma_1(\xi, \pm 1) = \sigma_0(\infty) = A \quad (\xi \to \infty). \tag{2.29a,b}$$

Equations (2.28) and (2.29) have the solution

$$\sigma_1(\xi, \eta) \sim A \quad (\xi \to \infty) \tag{2.30}$$

and hence

$$\sigma(\xi, \eta) \to 0 \quad (\xi \to \infty). \tag{2.31}$$

That is, the net displacement is zero, in sharp contrast to the two-dimensional solution. The two-dimensional solution is hence not a good approximation, at least sufficiently far downstream of the obstacle.

We now proceed to determine the finite value of $\sigma(\xi, \eta)$. For the reasons previously mentioned, we calculate the *maximum* value of $\sigma(\xi, \eta)$ as a function of $N$, concentrating on the limit

$$\epsilon \ll 1, \tag{2.32}$$

since in Boyer's experiments, $\epsilon$ was 0·0725.

Let $\hat{\psi}(k)$ denote the Fourier transform with respect to $\xi$ of any function $\psi(\xi)$, that is

$$\hat{\psi}(k) = \int_{-\infty}^{\infty} \psi(\xi)\, e^{ik\xi}\, d\xi, \tag{2.33}$$

where we extend the definition of the Fourier transform to include generalized transforms of the class described, for example, by Lighthill (1958). Fourier transforming (2.25) and (2.26), we obtain

$$(\partial_{\eta\eta}^2 - \kappa^2)\, \hat{\sigma}_1 = 0, \tag{2.34}$$

$$\hat{\sigma}_1(k, \pm 1) = \hat{\sigma}_0 = i\hat{M}(k)/[k(1 - ikN)]^{-1}, \tag{2.35a,b}$$

where (2.35*b*) is obtained by taking the Fourier transform of (2.21) and

$$\kappa = k/\epsilon. \tag{2.36}$$

Equations (2.34) and (2.35) have solution

$$\hat{\sigma}_1(k, \eta) = \frac{i\hat{M}(k)}{k(1 - ikN)} \frac{\cosh \kappa\eta}{\cosh \kappa} \tag{2.37}$$

and hence

$$\sigma_1(\xi, \eta) = \frac{1}{2\pi} \int_{-\infty}^{\infty} \frac{i\hat{M}(k)}{k(1 - ikN)} \frac{\cosh \kappa\eta}{\cosh \kappa} e^{-ik\xi}\, dk \tag{2.38}$$

$$= \epsilon \int_{-\infty}^{\infty} \sigma_0(\xi - t) \frac{\cos(\frac{1}{2}\pi\eta) \cosh(\frac{1}{2}\pi\epsilon t)\, dt}{\cos \pi\eta + \cosh \pi\epsilon t}, \tag{2.39}$$

where (2.39) follows from (2.38) on using the convolution theorem for Fourier transforms and the Fourier transform of $\cosh(\kappa\eta)/\cosh \kappa$ given in Erdélyi *et al.* [1954, §1.9 (12)].

In principle we now have the complete solution, since (2.23) can be integrated to determine $\sigma_0(\xi)$ and the result substituted into the right-hand side of (2.39). In practice, however, the solution $\sigma(\xi, \eta)$ cannot be represented in terms of simple, well-known functions. We thus concentrate on calculating a value for $\sigma$ that can be compared with Boyer's experiment and describe the flow in broad terms rather than with intricate formulae.

Considering that the *net streamline* displacement is zero, we feel that the maximum deviation of a streamline in the central part of the channel is a reasonable figure to compare with Boyer's experiments. The arguments behind such a statement are strengthened by the fact that Boyer's experimental results were less than his theoretical ones and he is hence likely to have carefully guarded against underestimating the measured displacement. We thus wish to evaluate the difference between $\sigma$ at two points, say $\xi_A(\eta)$ and $\xi_B(\eta)$, at which $\partial_\xi \sigma(\xi, \eta) = 0$.

Therefore, we first seek the values of $\xi$ such that

$$\sigma_0'(\xi) = \partial_\xi \sigma_1(\xi, \eta). \tag{2.40}$$

We determine the left-hand side of (2.40) by first integrating (2.22) to obtain

$$\sigma_0(\xi) = \int_{-\infty}^{\xi} M(t)\,dt - e^{-\xi/N} \int_{-\infty}^{\xi} e^{t/N} M(t)\,dt. \tag{2.41}$$

This expression can be simplified for $|\xi| \geqslant 1$ in that

$$\sigma_0(\xi) = \begin{cases} 0 & (\xi \leqslant -1), \qquad (2.42a) \\ A - Be^{-\xi/N} & (\xi \geqslant 1), \qquad (2.42b) \end{cases}$$

where

$$B = \int_{-1}^{1} e^{t/N} M(t)\,dt. \tag{2.43}$$

Anticipating that one of the $\xi$, say $\xi_B$, exceeds 1, we write the left-hand side of (2.40) as

$$(B/N)\,e^{-\xi/N}. \tag{2.44}$$

We determine the right-hand side of (2.40) by differentiating (2.38) to obtain

$$\partial_\xi \sigma_1(\xi, \eta) = \frac{\epsilon}{2\pi} \int_{-\infty}^{\infty} \frac{\hat{M}(\epsilon\kappa)}{1 - i\epsilon\kappa N} \frac{\cosh \kappa\eta}{\cosh \kappa} e^{-i\epsilon\kappa\xi}\,d\kappa \tag{2.45}$$

$$= \frac{\epsilon A}{2\pi} \int_{-\infty}^{\infty} \frac{\cosh \kappa\eta}{\cosh \kappa} d\kappa\,[1 + O(\epsilon^2, \epsilon^2\xi^2)] \tag{2.46a}$$

$$= \tfrac{1}{2}\epsilon A \sec \tfrac{1}{2}\pi\eta\,[1 + O(\epsilon^2, \epsilon^2\xi^2)], \tag{2.46b}$$

where the fact that $\hat{M}(0) = A$ has been used in deriving (2.46$a$) and the error terms in (2.46) are obtained assuming that $M(\xi)$, and hence $\hat{M}(k)$, is an even function. Equating (2.44) and (2.46$b$), we see that, for small $\epsilon$, $\xi_B$ is given by

$$\xi_B(\eta) = -N[\log \epsilon + \log (NA \sec \tfrac{1}{2}\pi\eta/2B)\,[1 + O(\epsilon^2 \log^2 \epsilon)], \tag{2.47}$$

and for the central part of the channel

$$\xi_B(0) = -N[\log \epsilon + \log (NA/2B)\,][1 + O(\epsilon^2 \log^2 \epsilon)]. \tag{2.48}$$

Substituting (2.48) into (2.42$b$), we obtain

$$\sigma_0[\xi_B(0)] = A(1 - \tfrac{1}{2}\epsilon N)\,[1 + O(\epsilon^2 \log^2 \epsilon)]. \tag{2.49}$$

We determine the value of $\sigma_1[\xi_B(0)]$ by setting $\eta = 0$ in (2.39) and introducing a change of variables in the integration to obtain

$$\sigma_1(\xi, 0) = \tfrac{1}{2}\epsilon \int_{-1}^{\infty} \sigma_0(t) \operatorname{sech} [\tfrac{1}{2}\epsilon\pi(\xi - t)]\,dt \tag{2.50}$$

$$= \tfrac{1}{2}\epsilon \int_{-1}^{1} \sigma_0(t)\,dt + \tfrac{1}{2}\epsilon A \int_{1}^{\infty} \operatorname{sech} [\tfrac{1}{2}\epsilon\pi(\xi - t)]\,dt$$

$$- \tfrac{1}{2}\epsilon B \int_{1}^{\infty} e^{-t/N} \operatorname{sech} [\tfrac{1}{2}\epsilon\pi(\xi - t)]\,dt + O(\epsilon^3, \epsilon^3\xi^3), \tag{2.51}$$

where (2.42) has been used in deriving (2.51) from (2.50). The second term in (2.51) equals

$$\tfrac{1}{2}A + \tfrac{1}{2}\epsilon A(\xi - 1) + O(\epsilon^3, \epsilon^3\xi^3)$$

and the third term equals $-\tfrac{1}{2}\epsilon BN + O(\epsilon^3, \epsilon^3\xi^3)$.

Thus
$$\sigma_1(\xi, 0) = \tfrac{1}{2}A + \tfrac{1}{2}\epsilon\left[A(\xi - 1) - BN + \int_{-1}^{1} \sigma_0(t)\,dt\right] + O(\epsilon^3, \epsilon^3\xi^2) \tag{2.52}$$

and

$$\sigma_1[\xi_B(0), 0] = \tfrac{1}{2}A - \tfrac{1}{2}AN\epsilon\log\epsilon - \frac{1}{2}\left[A + BN + AN\log(NA/2B) - \int_{-1}^{1} \sigma_0(t)\,dt\right]\epsilon + O(\epsilon^3\log^2\epsilon). \tag{2.53}$$

In a similar fashion we determine that

$$\xi_A(0) = -1 + O(\epsilon^{\frac{1}{2}}), \quad \sigma_0[\xi_A(0)] = O(\epsilon^{\frac{3}{2}}) \tag{2.54), (2.55}$$

and
$$\sigma_1[\xi_A(0), 0] = \tfrac{1}{2}A - \frac{1}{2}\left[BN - \int_{-1}^{1} \sigma_0(t)\,dt\right]\epsilon + O(\epsilon^{\frac{5}{2}}), \tag{2.56}$$

where the error terms in (2.54)–(2.56) have been obtained by assuming that

$$M(\xi) \sim M(-1) + (\xi + 1)\,M'(-1) \quad (\xi \downarrow -1), \tag{2.57}$$

with at least one of $M(-1)$ and $M'(-1)$ non-zero. Defining

$$\Delta\sigma(0) \equiv \sigma[\xi_B(0), 0] - \sigma[\xi_A(0), 0], \tag{2.58}$$

we use (2.25), (2.49), (2.53), (2.55) and (2.56) to obtain

$$\Delta\sigma(0) = A\{1 + \tfrac{1}{2}N\epsilon\log\epsilon - \tfrac{1}{2}[N + 1 - N\log(NA/2B)]\epsilon\} + O(\epsilon^{\frac{3}{2}}). \tag{2.59}$$

This expression for $\Delta\sigma(0)$ is plotted against the Rossby number in figures 2–5 for different values of the Ekman number for the triangle

$$M(\xi) = (1 - \xi\,\mathrm{sgn}\,\xi)\,H(1 - |\xi|), \tag{2.60}$$

for which $A = 1$ and $B = 4N^2\sinh^2(\tfrac{1}{2}N^{-1})$, and for the step

$$M(\xi) = H(1 - |\xi|), \tag{2.61}$$

for which $A = 2$ and $B = 2N\sinh(N^{-1})$. Also plotted on these figures are Boyer's experimental results. Those presented in figures 4 and 5, for the step (2.61), were obtained by Boyer to accompany the analysis (Boyer 1971*b*) which incorporates the $E^{\frac{1}{4}}$ inertial layers above the discontinuity at $\xi = \pm 1$. While these layers are necessary for a thoroughly detailed investigation of the flow, they can do no more than smooth the transition above the edges of the step to yield the flow field we have calculated; indeed the purpose of the inertial layers is to provide just such a smooth transition.

While the theory presented here results in a decrease of the streamline displacement with Rossby number as indicated by Boyer's experiments, the quantitative agreement with his results can only be described as fair. This is because using (2.1), which has error $O(E^{\frac{1}{2}})$, to describe a flow in the limit $\epsilon \to 0$ can only be valid if

$$E^{\frac{1}{2}} \ll \epsilon \ll 1. \tag{2.62$a$,$b$}$$

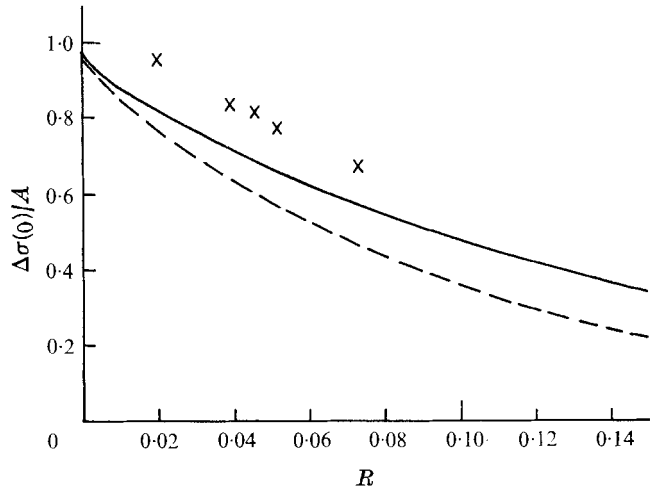


FIGURE 2. The normalized maximum streamline displacement in the central part of the channel as a function of Rossby number for flow over a triangular obstacle ($A = 1$) with $E = 9{\cdot}0 \times 10^{-4}$, $\epsilon = 0{\cdot}0725$, $h_0/D = 0{\cdot}063$ and $H/D = 0{\cdot}75$. ×, Boyer's experimental values; – – –, solution (2.59); ——, solution (3.9). Multiplication of the ordinate by $Y = 3{\cdot}78$ yields the streamline displacement in Boyer's experiment in cm.

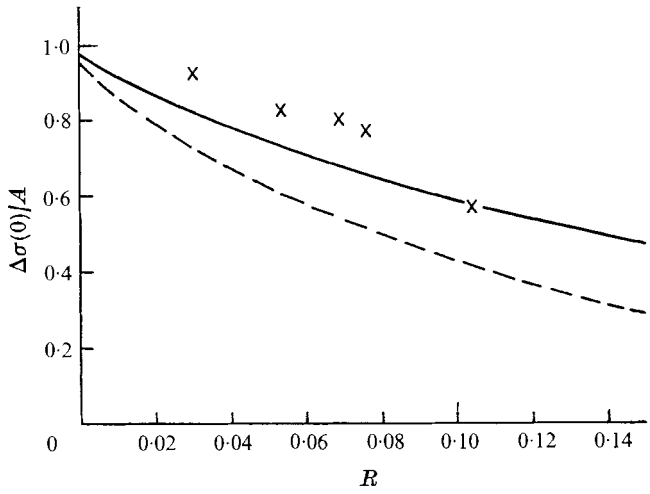


FIGURE 3. The streamline displacement as in figure 2, except that $E = 13{\cdot}3 \times 10^{-4}$ and $Y = 3{\cdot}10$.

In the experiments, $\epsilon = 0{\cdot}0725$ while $E^{\frac{1}{2}}$ was 0·030, 0·036 and 0·042. Thus (2.62$a$) was not well satisfied. In the next section we obtain a theory valid for

$$E^{\frac{1}{2}} \sim \epsilon \ll 1 \qquad (2.63a, b)$$

and show that this gives improved agreement between theory and experiment.

The simple theory presented in this section describes the major physical effect of the end walls. If the obstacle is very long compared with its breadth the flow in the centre of the channel is almost two-dimensional with a negative

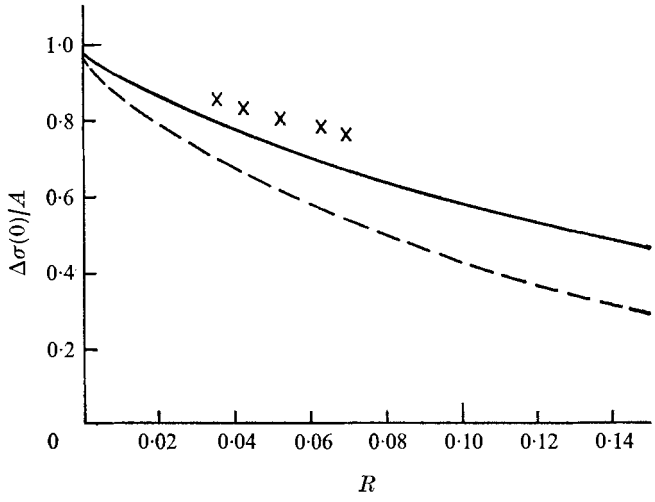


FIGURE 4. The streamline displacement as in figure 2, except that the flow is over a rectangular obstacle ($A = 2$) with $E = 13{\cdot}3 \times 10^{-4}$, $h_0/D = 0{\cdot}33$ and $Y = 1{\cdot}64$.

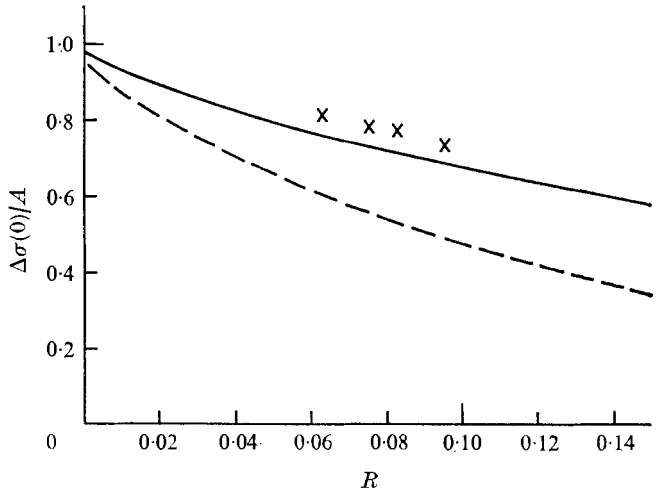


FIGURE 5. The streamline displacement over a rectangular obstacle as in figure 4, except that $E = 17{\cdot}9 \times 10^{-4}$ and $Y = 1{\cdot}40$.

cross-channel velocity above and for some distance downstream of the obstacle; see (2.41) and (2.42). This velocity, however, cannot be continued up to the end walls, at which the velocity must be zero. This is accomplished by an irrotational, three-dimensional flow which has a small, but significant effect in the centre of the channel, both up- and downstream of the obstacle. A central streamline drifts slowly to the left owing to the irrotational part of the flow upstream of the obstacle, arriving at the upstream edge having been displaced to the left by half the amount that the two-dimensional flow by itself would be displaced to the right in its motion from far upstream to far downstream [$\sigma(-1, 0) \sim -\frac{1}{2}A$]. The length scale relevant to this upstream part of the flow is $L$. The streamline

then turns sharply to the right on a length scale $D$, under the influence primarily of the rotational part of the solution. With passage downstream, the rotational flow decreases, to be overcome by the irrotational flow, which gradually takes the streamline back in line with its original position.

## 3. The solution for $E^{\frac{1}{2}} \sim \epsilon \ll 1$

*An outline of the calculation and the results*

Solving the lowest order vorticity equation (2.11) in the limit $\epsilon \to 0$ yields the simplest description incorporating the effects of the end walls that can be compared with the results of Boyer's experiments. Such a procedure, however, assumes that $E^{\frac{1}{2}} \ll \epsilon$, and it is the inaccuracy of this statement which is the major cause of the quantitative disagreement between the results of the previous section and Boyer's experiment. We remedy this by obtaining the lowest order solution in the limit

$$E^{\frac{1}{2}} \sim \epsilon \ll 1.$$

The concepts behind the calculation are as follows. An ordered expansion in terms of $E^{\frac{1}{2}}$ of the full Navier–Stokes equation can be written as

$$\sigma(\xi,\eta) = \sigma_0^{(0)}(\xi) + E^{\frac{1}{2}}\sigma_0^{(1)}(\xi) + \ldots - \sigma_1^{(0)}(\xi,\eta) - E^{\frac{1}{2}}\sigma_1^{(1)}(\xi,\eta) + \ldots + E^{\frac{1}{2}}\sigma_D^{(1)}(\xi) + \ldots, \quad (3.1)$$

where each function $\sigma$ is $O(1)$ with respect to $E^{\frac{1}{2}}$, but not necessarily $\epsilon$. Further, $\sigma_0^{(0)}$ and $\sigma_1^{(0)}$ are the $\sigma_0$ and $\sigma_1$ of the previous section and $\sigma_D^{(1)}(\xi)$ represents the drift, to the right across the channel, which exists to balance the transport to the left in the Ekman layers on the horizontal bounding surface and is given by†

$$\sigma_D^{(1)}(\xi) = \frac{D^2}{2H(E^{-\frac{1}{2}}h_0)}\xi \equiv \alpha\xi. \quad (3.2a,b)$$

Following the procedure of the previous section, we determine $\xi_B(0)$ by differentiating (3.1) with respect to $\xi$ and equating the result to zero, to obtain

$$\sigma_0^{(0)\prime}(\xi) + E^{\frac{1}{2}}\sigma_0^{(1)\prime}(\xi) + \ldots - \partial_\xi\sigma_1^{(0)}(\xi,0) - E^{\frac{1}{2}}\partial_\xi\sigma_1^{(1)}(\xi,0) + \ldots + E^{\frac{1}{2}}\sigma_D^{(1)\prime}(\xi) + \ldots = 0 \quad [\xi = \xi_B(0)]. \quad (3.3)$$

In the previous section, only the zeroth-order terms were considered, so that (3.3) was written as

$$\sigma_0^{(0)\prime}(\xi) - \partial_\xi\sigma_1^{(0)}(\xi,0) \quad [\xi = \xi_B(0)] \quad (3.4)$$

and both terms in (3.4) were $O(\epsilon)$. Thus, we anticipate the terms in (3.3) to be of order

$$\epsilon, E^{\frac{1}{2}}\epsilon, \ldots, \quad \epsilon, E^{\frac{1}{2}}\epsilon, \ldots, \quad E^{\frac{1}{2}}, \ldots.$$

† The form of this Ekman drift means that the definition of $S(x,y)$, or $\sigma(\xi,\eta)$, as the cross-channel streamline displacement from its *original* upstream position will have to be discarded. Since, however, it is really only differences in $S$ or $\sigma$ that concern us here, we neglect any constant that might be added to the right-hand side of (3.2).

Hence, to lowest order with $E^{\frac{1}{2}} \sim \epsilon$, $\xi_B(0)$ is determined from

$$\sigma_0^{(0)\prime}(\xi) - \partial_\xi \sigma_1^{(0)}(\xi, 0) + E^{\frac{1}{2}} \sigma_D^{(1)\prime}(\xi) = 0 \quad [\xi = \xi_B(0)]. \tag{3.5}$$

Similarly we calculate $\xi_A(0)$, which to lowest order will be given by

$$\xi_A(0) = -1.$$

These two values of $\xi$ are then substituted into (3.1), and the results subtracted to determine $\Delta\sigma(0)$, defined by (2.58). Writing $\Delta\sigma(0)$ in the format of (3.1), the order of the terms will be

$$1, E^{\frac{1}{2}}, \ldots, \quad \epsilon, \epsilon E^{\frac{1}{2}}, \ldots, \quad E^{\frac{1}{2}}, \ldots.$$

Hence

$$\Delta\sigma(0) \simeq \sigma_0^{(0)}[\xi_B(0)] + E^{\frac{1}{2}}\sigma_0^{(1)}[\xi_B(0)] - \sigma_1^{(0)}[\xi_B(0), 0] + \sigma_1^{(0)}(-1, 0) + E^{\frac{1}{2}}\sigma_D^{(1)}[\xi_B(0)] - E^{\frac{1}{2}}\sigma_D^{(1)}(-1), \tag{3.6}$$

where we have used the fact that

$$\sigma_0^{(0)}(-1) = \sigma_0^{(1)}(-1) = 0.$$

Given $\xi_B(0)$, equation (2.42*b*) can be used to determine $\sigma_0^{(0)}[\xi_B(0)]$, equation (2.52) can be used to determine both $\sigma_1^{(0)}[\xi_B(0), 0]$ and $\sigma_1^{(1)}(-1)$ and balancing the transport in the Ekman layer with that in the channel interior determines $\sigma_D^{(1)}(\xi)$. It remains only to determine $\sigma_0^{(1)}[\xi_B(0)]$, which equals $\sigma_0^{(1)}(\infty)$ to the order considered in (3.6). Thus we require the first-order final downstream displacement of the two-dimensional part of the solution.

The essential results of this calculation, which is presented below, are that

$$\xi_B(0) \simeq -N \log [N(\tfrac{1}{2}\epsilon A - \alpha E^{\frac{1}{2}})/B], \tag{3.7}$$

$$\sigma^{(1)}(\infty) = 0 \tag{3.8}$$

and

$$\Delta\sigma(0) \simeq A\{1 - (\tfrac{1}{2}\epsilon - \alpha E^{\frac{1}{2}}/A)[N + \xi_B(0) + 1]\}. \tag{3.9}$$

It is clear from (3.7) that these results can only be correct if

$$\epsilon E^{-\frac{1}{2}} > 2\alpha/A. \tag{3.10}$$

If (3.10) is not satisfied, the Ekman drift is sufficiently strong to cause the interior flow always to have a velocity component to the right, and hence there will be no point of maximum displacement. The result (3.8) reflects the fact that the first-order two-dimensional streamline displacement is zero and does not make a contribution to the maximum streamline displacement (3.9).

The evaluation of (3.8) with (3.7) using constants appropriate to Boyer's experiment leads to the curves plotted in figures 2–5. We see that there is agreement with Boyer's experimental results to within 10 %.

The streamline pattern is rather more complicated than that described in § 2. A consequence of the Ekman drift is that all interior streamlines emerge from the left-hand side-wall boundary layer and proceed across the channel to enter the right-hand side-wall boundary layer. The streamlines then return to the left-hand boundary layer via the Ekman layers on the horizontal surfaces.

Far upstream of the obstacle only the Ekman drift is significant and the streamlines move uniformly to the right. As the flow approaches the obstacle, the zeroth-order irrotational flow (2.39) increases in magnitude and there is a slow drift to the left given by

$$\sigma = (\alpha E^{\frac{1}{2}} - \tfrac{1}{2}\epsilon A)\,\xi. \tag{3.11}$$

Over the obstacle the flow is dominated by the zeroth-order rotational flow, described in § 2, which causes it to move to the right. Further downstream, there is still the gentle drift to the right described in § 2, though the magnitude is now slightly increased by the Ekman drift. For some distance downstream of the maximum point $\xi_B$, the streamlines verge to the left since the zeroth-order irrotational component exceeds the Ekman-drift component. The former, however, decreases with downstream distance and eventually the Ekman drift causes the flow to veer once more to the right.

*The first-order two-dimensional solution*

The two-dimensional Navier–Stokes equations are

$$2R(uu_\xi + wv_z) - v = -\Phi_\xi + 4E(u_{\xi\xi} + u_{zz}), \tag{3.12a}$$

$$2R(uu_\xi + wv_z) + u = -\epsilon\Phi_\eta + 4E(v_{\xi\xi} + v_{zz}), \tag{3.12b}$$

$$2R(uw_\xi + ww_z) = -\Phi_z + 4E(w_{\xi\xi} + w_{zz}), \tag{3.12c}$$

$$u_\xi + w_z = 0,$$

where the velocities have been non-dimensionalized with respect to $U$, $z$ is a vertical co-ordinate non-dimensionalized with respect to $\frac{1}{2}D$, and the non-dimensionalized pressure $\Phi = P/(\Omega UD)$. To (3.12) must be added the boundary conditions

$$u = v = w = 0 \quad [z = -2HD^{-1} + 2h_0 D^{-1}M(\xi)], \tag{3.13a,b,c}$$

$$u_z = v_z = w = 0 \quad (z = 0), \tag{3.14a,b,c}$$

$$u \sim 1, \quad v \sim 0 \quad (\xi \to -\infty). \tag{3.15a,b}$$

We determine the solution of (3.12)–(3.15) in the limit $R \sim E^{\frac{1}{2}} \to 0$ by matching the expansion of the interior solution to the expansion of the boundary-layer solution. The lowest order matching yields the lowest order vorticity equation [the two-dimensional version of (2.1)] and the next-order matching yields the next-order vorticity equation, from which $\sigma_0^{(1)}$ can be calculated.

*The interior solution.* Expanding all variables in a power series of $O(E^{\frac{1}{2}})$, equating like powers in $E^{\frac{1}{2}}$ and using the boundary conditions (3.14) and (3.15), we obtain the zeroth-order interior solutions

$$u^{(0)} = 1, \quad v^{(0)} = v^{(0)}(\xi), \quad w^{(0)} = 0, \tag{3.16a,b,c}$$

$$\Phi^{(0)} = -\epsilon^{-1}\eta + \psi^{(0)}(\xi); \tag{3.16d}$$

the first-order interior solutions

$$u^{(1)} = -av^{(0)\prime}(\xi), \quad v^{(1)} = \Phi^{(1)\prime}(\xi), \quad w^{(1)} = azv^{(0)\prime\prime}(\xi), \tag{3.17a,b,c}$$

$$\Phi^{(1)} = \Phi^{(1)}(\xi); \tag{3.17d}$$

and the second-order interior solutions

$$u^{(2)} = 4v^{(0)''}(\xi) - av_0^{(1)'}(\xi) + a^2[v^{(0)'}(\xi)]^2, \tag{3.18a}$$

$$v^{(2)} = \partial_\xi \phi^{(2)}(\xi, z) - a^2 v^{(0)''}(\xi), \tag{3.18b}$$

$$w^{(2)} = -z\{4v^{(0)'''}(\xi) - av_0^{(1)''}(\xi) + 2a^2 v_0^{(0)'}(\xi) v_0^{(0)''}(\xi)\}, \tag{3.18c}$$

$$\Phi^{(2)} = -\tfrac{1}{2}a^2 z^2 v^{(0)'''}(\xi) + \psi^{(2)}(\xi), \tag{3.18d}$$

where

$$a = 2RE^{-\frac{1}{2}} \tag{3.19}$$

is by hypothesis $O(1)$. Equations for the unknown functions $v^{(0)}(\xi)$ and $v^{(1)}(\xi)$ are determined by appropriately matching (3.16)–(3.18) to the boundary-layer solutions.

*The boundary-layer solution.* To determine the solution in the boundary layer at the bottom of the channel, boundary-layer variables

$$s = \xi, \quad t = E^{-\frac{1}{2}}[HD^{-1} + \tfrac{1}{2}z - h_0 D^{-1} M(\xi)] \tag{3.20a,b}$$

are introduced into (3.12) and (3.13), where $t$ is an appropriately stretched variable which takes the value zero at the bottom of the channel. Equations (3.12) and (3.13) then become, correct to within $1 + O(E)$,

$$2R[\tilde{u}\tilde{u}_s - M_0'(s)\,\tilde{u}\tilde{u}_t + \tfrac{1}{2}E^{-\frac{1}{2}}\tilde{w}\tilde{u}_t] - \tilde{v} = -\Phi_s + M_0'(s)\,\Phi_t + \tilde{u}_{tt}, \tag{3.21a}$$

$$2R[\tilde{u}\tilde{v}_s - M_0'(s)\,\tilde{u}\tilde{v}_t + \tfrac{1}{2}E^{-\frac{1}{2}}\tilde{w}\tilde{u}_t] + \tilde{u} = -\epsilon\Phi_\eta + \tilde{v}_{tt}, \tag{3.21b}$$

$$\tilde{u}_s - M_0'(s)\,\tilde{u}_t + \tfrac{1}{2}E^{-\frac{1}{2}}\tilde{w}_t = 0, \tag{3.21c}$$

$$\tilde{u} = \tilde{v} = \tilde{w} = 0 \quad (t = 0), \tag{3.22a,b,c}$$

where a tilde has been used to represent the boundary-layer value of a function,

$$M_0(\xi) = E^{-\frac{1}{2}}(h_0/D)\,M(\xi) \tag{3.23}$$

is a normalized representation of the obstacle and is by hypothesis $O(1)$, and the $z$ component of the momentum equations has been omitted since it is not needed. Expanding the unknown function as a power series in $E^{\frac{1}{2}}$ we obtain as the lowest order part of (3.21)

$$\tilde{v}^0 = v^{(0)} - \tilde{u}_{tt}^{(0)}, \quad \tilde{u}^{(0)} = 1 + \tilde{v}_{tt}^{(0)}, \tag{3.24a,b}$$

which with (2.22$a$, $b$) has the well-known solution

$$\tilde{u}^{(0)} = (1 - e^{-\tau}\cos\tau) - v^{(0)} e^{-\tau}\sin\tau, \tag{3.25}$$

$$\tilde{v}^{(0)} = e^{-\tau}\sin\tau + v^{(0)}(1 - e^{-\tau}\cos\tau), \tag{3.26}$$

where

$$\tau = t/2^{\frac{1}{2}}. \tag{3.27}$$

Substituting (3.25) into (3.12$c$) and using (3.22$c$), we obtain

$$\tilde{w}^{(0)} = 0 \tag{3.28}$$

and

$$\tilde{w}^{(1)} = 2M_0'(\xi) + 2^{\frac{1}{2}} v_s^{(0)}[1 - e^{-\tau}(\cos\tau + \sin\tau)]. \tag{3.29}$$

Equating terms $O(E^{\frac{1}{2}})$ in (3.21), we obtain

$$\tilde{u}_{tt}^{(1)} + \tilde{v}^{(1)} = v^{(1)} + a[\tilde{u}^{(0)}\tilde{u}_s^{(0)} - M_0'(\xi)\,\tilde{u}^{(0)}\tilde{u}_t^{(0)} + \tfrac{1}{2}\tilde{w}^{(1)}\tilde{u}_t^{(0)}], \tag{3.30}$$

$$\tilde{v}_{tt}^{(1)} - \tilde{u}^{(1)} = -u^{(1)} - av_s^{(0)} + a[\tilde{u}^{(0)}\tilde{v}_s^{(0)} - M_0'(\xi)\,\tilde{u}^{(0)}\tilde{v}_t^{(0)} + \tfrac{1}{2}\tilde{w}^{(1)}\tilde{v}_t^{(0)}]. \tag{3.31}$$

Substituting (3.25), (3.26) and (3.29) into (3.30) and (3.31), determining the solution of the resulting equations plus (3.22$a, b$), we substitute the result into (3.21$c$) and integrate with respect to $\eta$ between $\eta = 0$ and $\eta = \infty$ using (3.22$c$) to obtain

$$\tilde{w}^{(2)} \sim 2M_0'(\xi)\, u^{(1)} - 2^{\frac{3}{2}}[u_s^{(1)}(\tau - \tfrac{1}{2}) - \tfrac{1}{2}v_s^{(1)} + \tfrac{1}{2^0}\varpi_s] \quad (\eta \to \infty), \tag{3.32}$$

where $\varpi = a(9 + v^{(0)})\, v_s^{(0)}$.

*The matching.* The matching of the interior vertical velocity given by (3.17$c$) and (3.18$c$) to the boundary-layer vertical velocity given by (3.29) and (3.32) yields the equations from which the remaining unknown quantities can be determined. The lowest order matching of (3.17) and (3.29) leads to

$$-2a(H/D)\, v^{(0)''}(\xi) = 2M_0'(\xi) + 2^{\frac{1}{2}}v_\xi^{(0)'}. \tag{3.33}$$

Combining the two-dimensional versions of (2.7), (2.12) and (2.15), we can relate $v^{(0)}$ to $\sigma^{(0)}$ by

$$v^{(0)} = -2^{\frac{1}{2}}(h_0/DE^{\frac{1}{2}})\, \sigma_\xi^{(0)'}. \tag{3.34}$$

Substituting (3.34) into (3.33) and using (3.32), we see that (3.33) is equivalent to

$$(N\partial_\xi + 1)\, \partial_{\xi\xi}^2 \sigma^{(0)} = M'(\xi), \tag{3.35}$$

in agreement with (2.20).

The first-order matching, of (3.18$c$) and (3.32), leads to

$$2a\frac{H}{D}v^{(1)''}(\xi) + 2(v^{(1)'})^{\frac{1}{2}}(\xi) = \frac{8H}{D}v^{(0)'''}(\xi) + 4a^2\frac{H}{D}v^{(0)'}(\xi)\, v^{(0)''}(\xi) - 2[M_0(\xi)\, u^{(1)}(\xi)]' + 2^{\frac{1}{2}}av^{(0)''}(\xi) + 2^{\frac{3}{2}}\varpi(\xi). \tag{3.36}$$

To evaluate $\sigma_0^{(1)}(\xi)$, we first combine (2.7), (2.12) and (2.15) to obtain

$$\sigma_0(\xi) = -Dh_0^{-1}(\tfrac{1}{2}E)^{\frac{1}{2}}\int_{-\infty}^{\xi}(v/u)\, d\xi \tag{3.37a}$$

$$= -Dh_0^{-1}(\tfrac{1}{2}E)^{\frac{1}{2}}\left\{\int_{-\infty}^{\xi}v^{(0)}d\xi + E^{\frac{1}{2}}\int_{-\infty}^{\xi}(v^{(1)} - v^{(0)}u^{(1)})\, d\xi + O(E)\right\}. \tag{3.37b}$$

Thus

$$\sigma_0^{(1)}(\infty) = -[Dh_0^{-1}(\tfrac{1}{2}E)^{\frac{1}{2}}]\int_{-\infty}^{\infty}(v^{(1)} - v^{(0)}u^{(1)})\, d\xi. \tag{3.38}$$

The integral of $v^{(1)}$ can be determined by integrating (3.36) between $-\infty$ and $\xi$ and integrating the result between $-\infty$ and $+\infty$ to obtain

$$2^{\frac{1}{2}}\int_{-\infty}^{\infty}v^{(1)}\, d\xi = \int_{-\infty}^{\infty}[2a^2HD^{-1}(v^{(0)'})^2 - 2M_0u^{(1)}]\, d\xi \tag{3.39a}$$

$$= 2a\int_{-\infty}^{\infty}v^{(0)'}[aHD^{-1}v^{(0)'} + M_0]\, d\xi \tag{3.39b}$$

$$= 2^{\frac{1}{2}}a\int_{-\infty}^{\infty}v^{(0)'}v^{(0)}\, d\xi \tag{3.39c}$$

$$= 0, \tag{3.39d}$$

since $v^{(0)}(\pm\infty) = 0$, where (3.17$a$) and (3.33) have been used in reducing (3.39$a$) to (3.39$d$). Using (3.17$a$), we see also that

$$\int_{-\infty}^{\infty} v^{(0)} u^{(1)}\, d\xi = 0, \tag{3.40}$$

and hence

$$\sigma_0^{(1)}(\infty) = 0. \tag{3.41}$$

The first-order, net, two-dimensional streamline displacement is thus identically zero.

## 4. Conclusions

We conclude that side walls play a most significant role in determining the flow over a long obstacle in a rotating system. Eliminating the effect of the interior Ekman drift, as can be achieved, for example, by towing the obstacle with speed $U$ through an otherwise quiescent fluid, we find that the net lateral displacement of a column of fluid after passage over an obstacle of constant cross-section is zero. This result is in sharp contrast with that obtained by neglecting the side walls, in which case the lateral displacement monotonically increases with downstream distance to a final value independent of the Rossby number and given by (1.6). As shown in §2, the presence of vertical boundaries introduces an irrotational flow forced at the side walls which is of just the correct magnitude to cancel the contribution independent of the side walls far downstream.

The additional effect of the upstream Ekman drift, as discussed in §3, can be isolated by considering the flow in a bounded channel, in the absence of an obstacle. The Ekman transport to the left, which exists in the horizontal boundary layers, is then balanced solely by a continuous slow interior drift of the geostrophic flow to the right.

These two different effects of the side walls can be seen in figures 2–5, which depict the maximum lateral displacement as a function of the Rossby number. The broken curves, determined from (2.59), are valid for flow over a fixed obstacle with $E^{\frac{1}{2}} \ll \epsilon \ll 1$, or for the flow induced by a towed obstacle. The displacement so obtained decreases more strongly with increasing Rossby number than Boyer's experimental results. The addition of the interior Ekman drift leads to the solid lines given by (3.7) and (3.9). Agreement with Boyer's experimental results is now to within 10%, as good as might be expected considering the difficulty of the experiment and the fact that we have determined the displacement to lowest order.

Both authors gratefully acknowledge the support of the 1972 Geophysical Fluid Dynamics Summer Program at Woods Hole. H.E.H. is also thankful for the support of the British Admiralty and the office of Naval Research under Contract N00014-67-A-0204-0047.

## Appendix

The aim of this appendix is to prove the validity of the linearization of (2.10) to obtain (2.11). This is done by calculating the terms neglected in (2.10) using the solutions of (2.11) and proving that they are appropriately small. While such a procedure may not have the elegance of the more usual method of expanding the solutions of (2.10) as a power series in some small quantity, say $\delta$, and obtaining the solution of (2.11) as the first term in such an expansion, it is equally valid and in this case more direct.

To obtain (2.11), we have in essence linearized (2.7) to let

$$v = US_x. \tag{A 1}$$

From the equation of continuity, therefore,

$$u = U(1-S_y). \tag{A 2}$$

Since we have used $U$ in place of $u$ in (2.11), a necessary condition for the consistency of our approach is that

$$|S_y| \ll 1. \tag{A 3}$$

Explicitly, now, considering the first term of (2.11), we have retained

$$U^2\nabla^2 S_x \tag{A 4}$$

and neglected

$$U\nabla^2(\tilde{u}S_x) + U\tilde{u}\nabla^2 S_x + \tilde{u}\nabla^2(\tilde{u}S_x) + v\partial_y\nabla^2\left[US + \int_{-\infty}^{x}\tilde{u}S_x dx\right] \tag{A 5}$$

$$\simeq -2U^2 S_y \nabla^2 S_x(1-\tfrac{1}{2}S_y), \tag{A 6}$$

where we have written

$$u = U + \tilde{u} \tag{A 7}$$

in (A 5) and obtained (A 6) by using (A 1) and (A 2) for $u$ and $v$ and also the fact that $\nabla^2 S_y = 0$ [(2.20) and (2.25)]. A consequence of the last statement is that the $v\partial_y$ contribution of the $\mathbf{q}.\nabla$ operator in (2.10), that is, the square-bracketed term in (A 5), is zero. The terms of (A 6) will be negligible compared with that of (A 4) under the condition (A 3).

In the second term of (2.11), we have retained

$$Uh_x \tag{A 8}$$

and neglected

$$\tilde{u}h_x \simeq -US_y h_x. \tag{A 9}$$

Again this is valid if (A 3) is satisfied.

In the third term of (2.11), we have retained

$$U\nabla^2 S \tag{A 10}$$

and neglected

$$\nabla^2\int_{-\infty}^{x}\tilde{u}S_x dx \simeq -US_y\nabla^2 S. \tag{A 11}$$

Thus, (A 3) is a necessary and sufficient condition for the solutions of (2.11) to be an appropriate model of those of (2.10).

In terms of $\sigma(\xi, \eta)$, (A 3) becomes

$$\epsilon|\partial_\eta \sigma_1(\xi, \eta)| \ll 1. \tag{A 12}$$

We evaluate the left-hand side of (A 12) by differentiating (2.38) to obtain

$$\epsilon|\partial_\eta \sigma_1(\xi, \eta)| = \frac{\epsilon}{2\pi}\left|\int_{-\infty}^{\infty} \frac{iM(\epsilon\kappa)}{1 - i\epsilon\kappa N} \frac{\sinh \kappa\eta}{\cosh \kappa} e^{-i\epsilon\kappa\xi} d\kappa\right| \tag{A 13}$$

$$\sim \frac{\epsilon A}{2\pi}\left|\int_{-\infty}^{\infty} \frac{\sinh \kappa\eta}{\cosh \kappa} e^{-i\epsilon\kappa\xi} dk\right| \quad (\epsilon \to 0) \tag{A 14}$$

$$= \tfrac{1}{2}\epsilon A \frac{\sin(\frac{1}{2}\pi\eta) \sinh(\frac{1}{2}\epsilon\pi\xi)}{\cosh \epsilon\pi\xi + \cosh \pi\eta} \tag{A 15}$$

$$= O(\epsilon). \tag{A 16}$$

Thus the solutions of (2.11) equal those of (2.10) to within an error factor that is uniformly of order $\epsilon$.

## REFERENCES


Boyer, D. L. 1971*a* Rotating flow over long shallow ridges. *Geophys. Fluid Dyn.* **3**, 165–184.

Boyer, D. L. 1971*b* Rotating flow over a step. *J. Fluid Mech.* **50**, 675–687.

Boyer, D. L. & Guala, J. R. 1972 Model of the Antarctic Circumpolar Current in the vicinity of the Macquarie Ridge. *Am. Geophys. Un., Antartic Res. Ser.* **19**, 79–93.

Erdélyi, A., Magnus, W., Oberhettinger, F. & Tricomi, F. S. 1954 *Tables of Integral Transforms*, vol. 1. McGraw-Hill.

Greenspan, H. 1968 *The Theory of Rotating Fluids*. Cambridge University Press.

Greenspan, H. P. & Howard, L. N. 1963 On the time-dependent motion of a rotating fluid. *J. Fluid Mech.* **17**, 385–404.

Ingersoll, A. R. 1969 Inertial Taylor columns and Jupiter's Great Red Spot. *J. Atmos. Sci.* **26**, 744–752.

Lighthill, M. J. 1958 *Fourier Analysis and Generalized Functions*. Cambridge University Press.